Extended Abstract: Adaptive LiDAR Inertial Odometry with an Ellipsoid Representation (EllipseLIO)

Rowan Border [1] and Margarita Chli [1]

***Abstract*— LiDAR Inertial Odometry (LIO) is a critical component for many mobile robots that navigate without external positioning. Existing LIO approaches can provide reliable odometry in many scenarios when suitably tuned but often struggle to generalise between heterogeneous environments and sensors. This work presents EllipseLIO, a real-time LIO approach that leverages adaptive methods for scan filtering and registration to provide robust odometry across different scenarios without requiring specific tuning. Experiments on five diverse and challenging datasets show that EllipseLIO is the best-performing approach overall. It achieves a 38% lower odometry error on average than the second-best approach and is the only approach that does not diverge on any sequence.**

I. Introduction

Reliable odometry is essential for autonomous platforms that need to operate in challenging environments without external positioning (e.g., GPS/GNSS). LiDAR Inertial Odometry (LIO) approaches provide real-time pose estimation onboard platforms by combining high-fidelity geometric measurements from a LiDAR and high-frequency motion estimates from an Inertial Measurement Unit (IMU). For a LIO approach to provide robust odometry on heterogeneous autonomous platforms (e.g., aerial, ground-based, and waterborne) that operate in diverse environments (e.g., small enclosed structures, large open areas, and unstructured natural scenes) using different sensors, it must adapt to each scenario without human intervention.

Existing LIO approaches can provide accurate odometry in homogeneous scenarios, with similar environments and sensors, but typically do not generalise well between different scenarios. Many approaches use fixed-resolution scan filtering, which can produce scans that are too sparse for accurate registration in small-scale environments or too dense for real-time processing in large-scale environments. Most use scan registration methods with fixed error metrics that make planar surface assumptions, which can cause accuracy to degrade in unstructured environments where these assumptions are invalid. This lack of adaptability produces variations in the odometry performance between different scenarios (Fig. 1) and sometimes results in divergence.

The approach presented in this work, *EllipseLIO*, addresses these challenges with three key contributions: (i) a range-based scan filter that adaptively varies the downsampling resolution; (ii) an ellipsoid-based scan registration method that adapts the error metrics used to the local surface geometry; and (iii) drift correction that is directly integrated into the scan registration, via adaptive weighting of point matches, and does not require explicit loop closure handling.

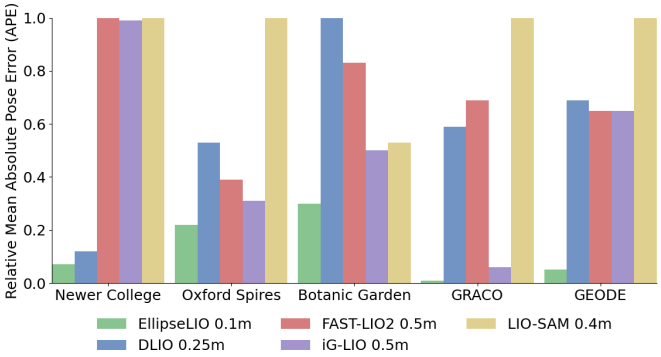

Fig. 1. Results for EllipseLIO and the compared LIO approaches on five datasets with heterogeneous scenarios. The Relative Mean APE is defined as the mean APE of an approach on a dataset divided by the greatest mean APE from all of the approaches, such that the values are scaled to $(0, 1]$. EllipseLIO is consistently the best-performing approach, while the relative performance of the compared approaches varies between the datasets.

II. Related Work

LIO approaches typically consist of three stages: scan preprocessing, scan registration, and map update.

1) Scan Preprocessing: Raw LiDAR scans contain over a hundred thousand points and must be reduced for real-time processing. Feature-based approaches [1–3] extract lines and planes but typically do not generalise between different sensors. Voxel downsampling [4–6] is efficient, but a fixed resolution does not adapt to environment scale or sensor capabilities. AdaLIO [7] switches between resolutions based on the environment scale but requires heuristic tuning. The presented approach adaptively varies the downsampling resolution used at different ranges based on the LiDAR field-of-view and resolution to retain more geometric information.

2) Scan Registration: Most LIO approaches use Iterative Closest Point (ICP) variants [4–6] for scan-to-map registration. Point-to-plane ICP converges efficiently in structured environments but can degrade in unstructured environments where planar assumptions are invalid. Generalised ICP [8] reduces sensitivity to sensor noise but still makes planar surface assumptions. Super Odometry [9] and GenZ-ICP [10] reduce drift and prevent divergence by combining multiple registration metrics using weights derived from threshold parameters. The presented ellipsoid-based registration method adapts the error metric used for each map point based on weights obtained directly from its associated ellipsoid.

3) Map Update: The map update aggregates points from LiDAR scans into a map with a common reference frame that

[1] Authors are with the Vision for Robotics Lab (V4RL), University of Cyprus, Cyprus and ETH Zurich, Switzerland.

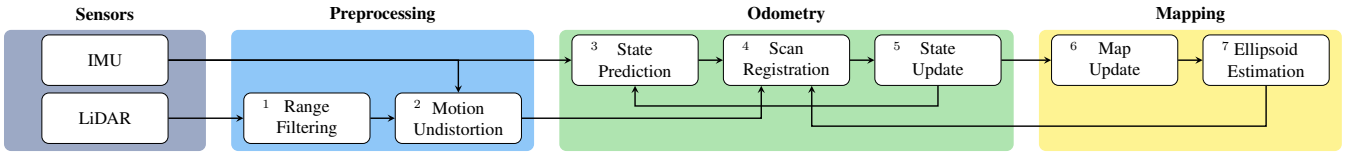

Fig. 2. The EllipseLIO pipeline: (1) LiDAR scans are range-filtered and (2) motion-undistorted. (3) IMU measurements propagate state predictions, while (4) the filtered scan is registered to the ellipsoid map to obtain a pose estimate, and (5) the odometry state is updated. (6) The map is updated with new points, and (7) ellipsoids are initialised or updated to reflect the local surface geometry.

can be used for scan-to-map registration. Most approaches use data structures like ikd-trees [3, 4], Octrees [11], or voxel hash maps [6] for efficient point management. Some methods also integrate higher-level representations (e.g., surfels [11, 12]) to capture additional geometric detail. EllipseLIO uses an iOctree [13] data structure with an ellipsoid-based map representation to provide high-fidelity geometric information.

III. EllipseLIO

Figure 2 presents the EllipseLIO pipeline. LiDAR scans are preprocessed with motion undistortion and adaptive range-based filtering. The filtered scans are then processed by the odometry pipeline to perform state estimation with an iterated Extended Kalman Filter (iEKF) [3]. The state is updated by registering scans against the map with ellipsoid-based registration metrics and propagated between scans using the high-frequency IMU measurements. The registered scans are aggregated into a globally consistent iOctree [13] and the ellipsoid map representation for new and existing points is updated using the method presented in [14].

A. Adaptive Range-Based Filtering

Uniform voxel downsampling at a fixed resolution does not generalise well between different environment scales. A high resolution is most suitable for narrow indoor areas but produces prohibitively dense scans in large open areas, while using a lower resolution that is suitable for large open spaces can discard too much geometric information. EllipseLIO addresses this challenge by partitioning LiDAR scans into 1 m wide radial bins and applying a different downsampling resolution to each bin. The resolution for bin i is given by the separation distance between the scan lines at range $i+1$,

$$v_i = \frac{(i+1)\,\theta}{\beta - 1}\,, \tag{1}$$

where θ is the vertical field-of-view of the LiDAR and β is the number of scan lines. Each bin is downsampled with an iOctree voxel filter at resolution v_i, and the filtered pointclouds from each bin are combined. This method retains denser measurement coverage on nearby surfaces and sparser coverage on distant ones, providing a spatially balanced point distribution that supports accurate registration across different environment scales without parameter retuning.

B. Ellipsoid-Based Scan Registration

Each scan point in the global frame, ${}^{G}\mathbf{p}$, is matched with its closest map point, ${}^{G}\mathbf{q}$, by performing a nearest-neighbour search within a given radius, which varies with the range of the scan point. The registration error metric used for

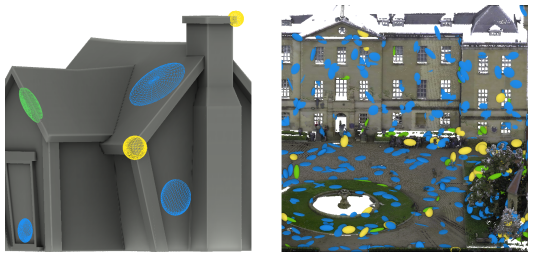

Fig. 3. Illustrated (left) and real (right) ellipsoids classified by their most salient geometric primitive: *lines* (green), *planes* (blue), and *balls* (yellow). The ellipsoids adapt the registration metric to the local surface geometry.

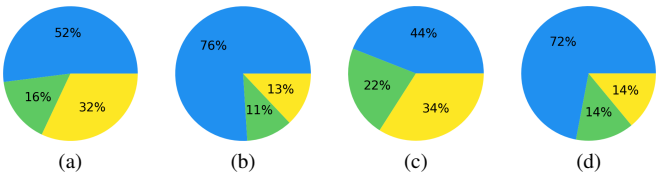

Fig. 4. The distribution of ellipsoid classifications, as planes (blue), lines (green), and balls (yellow), for (a) *parkland-mound*, (b) *observatory-01*, (c) *1006-01*, and (d) *aerial-04*. The change in classifications between structured (b, d) and unstructured (a, c) environments shows how variations in the surface geometry are captured by the ellipsoid representation.

each match is determined by the structure of the ellipsoid associated with the map point. This structure is decomposed into geometric primitives representing *lines*, *planes*, and *balls* (Fig. 3). Line primitives denote surfaces with a single dominant axis of variation (e.g., a pole) and use a point-to-line metric. Plane primitives denote surfaces with minimal variation along a single axis (i.e., the surface normal) and use a point-to-plane metric. Ball primitives denote surfaces with similar variation along each axis and use a point-to-point metric. A saliency score for each primitive, $\mathbf{g} = [g_{\text{line}}, g_{\text{plane}}, g_{\text{ball}}]$, is directly obtained from the eigenvalues computed during the ellipsoid estimation without requiring any threshold parameters. The target point for a match, ${}^{G}\mathbf{p}'$, is the sum of the target points for each geometric primitive, weighted by their L1-normalised saliency scores,

$${}^{G}\mathbf{p}' = \frac{g_{\text{line}}}{||\mathbf{g}||_1}\,{}^{G}\mathbf{p}'_{\text{line}} + \frac{g_{\text{plane}}}{||\mathbf{g}||_1}\,{}^{G}\mathbf{p}'_{\text{plane}} + \frac{g_{\text{ball}}}{||\mathbf{g}||_1}\,{}^{G}\mathbf{p}'_{\text{ball}}\,. \tag{2}$$

C. Adaptive Match Weighting and Drift Correction

EllipseLIO integrates drift correction directly into the scan registration pipeline by adaptively weighting point matches to prioritise those with older ellipsoids when the sensor returns to a previously visited location. Each point match is weighted based on the distance traveled since the map point was captured. Map points with large travel distances

		Odometry Performance (APE RMSE in meters)				
		EllipseLIO	DLIO	FAST-LIO2	LIO-SAM	iG-LIO
	Voxel Resolution (m)	0.1	0.1 / 0.25	0.1 / 0.5	0.1 / 0.4	0.1 / 0.5
Newer College	short-experiment	**0.30**	0.45 / 0.44	× / 0.41	× / 0.41	0.51 / 0.34
	quad-with-dynamics	0.09	0.14 / 0.15	× / 0.12	**0.08** / **0.08**	0.09 / 0.09
	dynamic-spinning	**0.08**	0.15 / 0.15	× / **0.08**	0.10 / 0.10	**0.08** / 0.09
	parkland-mound	**0.12**	0.19 / 0.19	× / **0.12**	× / 0.13	× / 0.14
	stairs	**0.08**	**0.08** / 0.10	**0.08** / ×	2.68 / ×	× / ×
	cloister	**0.07**	0.21 / 0.20	× / 0.08	× / 0.12	0.26 / 0.12
	quad-hard	**0.07**	0.16 / 0.12	× / 0.11	1.49 / 0.12	× / 0.10
Oxford Spires	blenheim-01	0.14	0.46 / 0.31	× / 0.14	× / 0.52	× / **0.12**
	bodleian-02	**0.19**	0.75 / 0.54	× / 0.54	0.42 / 1.32	× / 0.32
	christchurch-03	**0.03**	0.08 / 0.07	× / 0.04	× / 0.08	× / 0.08
	keble-02	**0.05**	0.08 / 0.06	× / **0.05**	× / 0.13	0.13 / 0.07
	observatory-01	**0.06**	0.27 / 0.18	× / 0.08	× / 0.13	× / 0.09
Botanic Garden	1005-00	**0.23**	1.39 / 0.71	1.43 / 0.48	× / 0.47	2.41 / 0.28
	1005-01	0.17	0.47 / 0.56	0.55 / 0.37	0.38 / 0.37	1.13 / **0.13**
	1005-07	**0.36**	0.86 / 0.72	1.87 / 0.69	0.55 / 0.47	× / 0.71
	1006-01	**0.15**	1.37 / 1.15	0.46 / 1.23	× / 0.44	4.76 / 0.29
	1008-03	**0.24**	0.52 / 0.74	0.82 / 0.43	× / 0.30	2.03 / 0.54
GRACO	aerial-01	**0.20**	× / ×	× / ×	× / ×	× / 0.32
	aerial-02	**0.07**	× / 0.25	1.67 / ×	× / ×	× / 0.09
	aerial-03	**0.07**	× / ×	× / ×	× / ×	× / 0.18
	aerial-04	**0.12**	× / ×	× / ×	× / ×	× / 0.35
	aerial-05	**0.21**	× / ×	× / ×	× / ×	× / 1.77
	aerial-06	**0.07**	× / 0.14	1.68 / 1.49	× / ×	× / 1.09
	aerial-07	**0.09**	× / 6.71	1.59 / 1.74	× / ×	× / 1.00
	aerial-08	**0.13**	× / 0.24	1.00 / 1.93	× / ×	× / 0.21
GEODE	water-short-alpha	**0.54**	× / 2.56	× / ×	× / ×	× / ×
	water-short-beta	**0.26**	× / 0.64	× / 0.35	4.52 / 0.85	× / 0.33
	offroad1-alpha	**0.11**	× / ×	1.66 / 0.12	× / 0.18	× / **0.11**
	offroad1-beta	**0.14**	0.30 / 0.23	5.88 / 0.20	× / **0.14**	× / 0.15
	stairs-alpha	**0.23**	× / 8.63	× / ×	× / ×	× / ×
	stairs-beta	**0.09**	0.92 / 0.24	× / 0.28	5.62 / ×	× / 0.21
	tunnel3-alpha	0.20	**0.18** / **0.18**	1.22 / **0.18**	**0.18** / 1.26	× / **0.18**
	tunnel3-beta	**0.15**	0.19 / 0.19	1.80 / 0.20	× / 0.20	0.16 / **0.15**

Table 1. APE RMSE (m) for EllipseLIO (ours) and compared LIO approaches on five datasets. Best in **bold**, second-best underlined. Experiments with APE RMSE $\geq$ 10 m diverged and are marked ×. Each compared approach is run at a 0.1 m voxel resolution (left) and its best-tuned resolution (right). EllipseLIO consistently achieves the best or second-best result and never diverges.

indicate that the sensor has traveled farther and accumulated more odometry drift before returning to a previously visited location. Matches with these map points are assigned greater weight during the iEKF update to correct this drift.

The match weight w is given by the difference in trajectory length $\mathrm{s}(t)$ between the measurement time of the scan point $t_{\mathbf{p}}$, and its matched map point $t_{\mathbf{q}}$. Matches with error in the vertical axis, where drift typically accumulates faster due to fewer measurement constraints, are given greater weight,

$$w = \frac{\mathrm{s}(t_{\mathbf{p}}) - \mathrm{s}(t_{\mathbf{q}}) + 1}{\max\left(1 - |\widehat{\mathbf{t}} \cdot \widehat{\boldsymbol{\gamma}}|, 10^{-4}\right)}, \tag{3}$$

where $\mathbf{t} = {}^{G}\mathbf{p} - {}^{G}\mathbf{p}'$ is the translation vector from the target point to the scan point and $\widehat{\boldsymbol{\gamma}}$ is the unit gravity vector.

Large match weights can increase the risk of divergence in geometrically degenerate environments where some state dimensions are poorly constrained. EllipseLIO adapts the degeneracy detection method presented in SuperLoc [15] to estimate the level of degeneracy in the translation and rotation axes and scales the match weights to mitigate the risk of divergence. This ensures that small weights are applied when the geometry is degenerate and larger weights can be used when the sensor revisits a well-structured location.

D. Mapping

The mapping module aggregates registered LiDAR scans into a combined global map using an iOctree [13]. Ellipsoids are created for newly added map points and updated for existing map points in the local neighbourhood of newly added points using the Tensor Voting (TV) method presented in [14]. The relative positions of neighbouring points within a given radius of each point are encoded into a 2D tensor, which is eigendecomposed to obtain an initial estimate of the local surface normal. These initial estimates are propagated as tensor votes between the points and the final ellipsoid for each point is obtained by eigendecomposing a weighted sum of the tensor votes from its neighbouring points. EllipseLIO varies the point density and scale of ellipsoids based on their distance from the sensor to maintain a representation that supports accurate scan registration across varying ranges. This adaptive method ensures that nearby ellipsoids represent smaller, higher-resolution surface areas, while distant ellipsoids maintain a coarser representation to balance geometric fidelity with computational efficiency.

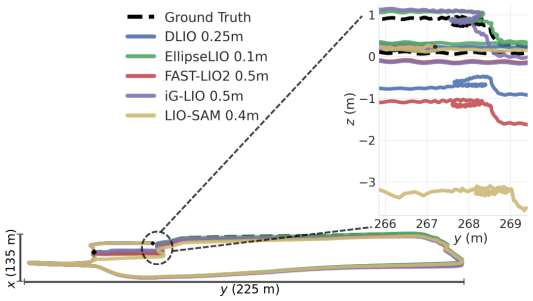

Fig. 5. The LIO approach trajectories on the *bodleian-02* sequence, showing their drift when aligned with the ground truth.

IV. Evaluation

A. Experimental Setup

EllipseLIO is evaluated on five datasets spanning a broad range of environments and platforms: Newer College [16, 17] and Oxford Spires [18], which contain mostly structured urban environments captured with a handheld platform; Botanic Garden [19], which captures a natural park environment with a wheeled platform; GRACO [20], which captures a university campus from an aerial platform flying at 20–40 m altitude; and GEODE [21], which contains indoor and outdoor environments captured from waterborne, handheld, and wheeled platforms.

EllipseLIO is compared with DLIO [5], FAST-LIO2 [4], LIO-SAM [2], and iG-LIO [6] using their open-source implementations. All of the approaches use fixed parameters for every sequence. The compared approaches are run with the same voxel resolution as EllipseLIO and their best-tuned resolution. Odometry accuracy is measured by Absolute Pose Error (APE) Root Mean Square Error (RMSE) after $\mathrm{SE}(3)$ Umeyama alignment with the ground truth trajectory [22].

B. Results

The odometry results (Table 1) show that EllipseLIO consistently attains the lowest or second-lowest APE across all sequences and achieves a 38% lower APE on average than the second-best approach, iG-LIO 0.5 m. EllipseLIO is also the only approach that does not diverge on any sequence.

	EllipseLIO	DLIO	FAST-LIO2	LIO-SAM	iG-LIO
Voxel Res. (m)	0.1	0.1 / 0.25	0.1 / 0.5	0.1 / 0.4	0.1 / 0.5
Comp. Time (ms)	35	33 / 34	203 / 51	157 / 91	31 / **11**
Memory (GB)	2.4	7.2 / 2.9	4.3 / 0.7	2.2 / 0.7	6.9 / **0.5**

Table 2. Mean computation time and memory usage on *parkland-mound*. Best **bold**, second-best underlined. Values for diverged approaches in gray and excluded. EllipseLIO runs in real time at a 4–5× finer map resolution than the lowest-memory approaches.

1) Unstructured Environments: The ellipsoid representation captures the shift in surface geometry between environments (Fig. 4). In natural environments (e.g., *1006-01* and *parkland-mound*) fewer than 55% of ellipsoids are primarily planar, compared with over 70% in structured environments. The adaptivity of EllipseLIO enables it to retain more consistent performance between different environments than the compared approaches. Its mean APE is only $2\times$ higher on the unstructured Botanic Garden dataset than on the structured Oxford Spires dataset, while DLIO, FAST-LIO2, and iG-LIO, which make planar surface assumptions, show a $3\times$ increase in mean APE.

2) Large-scale Open Environments: On the GRACO aerial sequences, where the drone flies at 20–40 m, the wide separation between scan lines creates highly non-uniform point distributions that corrupt fixed planar surface estimates, which causes every compared approach except iG-LIO to diverge on most sequences. The range-adaptive filtering used by EllipseLIO ensures that the distribution of points retained at different altitudes is appropriate for the sensor resolution.

3) Small-scale Enclosed Environments: In confined environments (e.g., *stairs*, *stairs-alpha*, and *stairs-beta*), most of the compared approaches with their tuned resolutions, except for DLIO on the *stairs* sequence, diverge or yield an APE more than twice that of EllipseLIO. This performance gap can be attributed to overly aggressive scan filtering that fails to retain sufficient measurements. Even when these approaches use a finer 0.1 m voxel resolution, many of them continue to diverge because their registration methods do not adjust the number of neighbouring points or voxels used for surface estimation to account for the increased point density.

4) Drift Correction: EllipseLIO mitigates drift upon returning to previously visited locations by adaptively weighting point matches during the scan registration. A comparison of trajectories on the *bodleian-02* sequence (Fig. 5) shows that EllipseLIO closely tracks the ground truth while the other approaches suffer from more pronounced drift.

5) Computational Performance: Table 2 shows the mean computation time and memory usage of the approaches on the *parkland-mound* sequence. EllipseLIO runs in real time at 35 ms per scan. DLIO 0.1 m is the only compared approach that completes this sequence when using the same resolution as EllipseLIO without diverging. It runs at similar speed to EllipseLIO but uses $3\times$ more memory. The higher memory usage of EllipseLIO reflects that it uses a 4–$5\times$ finer map resolution than the lowest-memory approaches.

V. Conclusion

EllipseLIO provides reliable odometry across diverse environments and heterogeneous sensors without scenario-specific tuning. It addresses key challenges for LIO approaches with adaptive range-based scan filtering, ellipsoid-based scan registration metrics that adapt to the surface geometry, and drift correction that is integrated directly into the registration pipeline. Experiments across 33 sequences on five datasets show that EllipseLIO achieves at least 29% lower APE on average for every dataset than the second-best approach, and it is the only approach that never diverges. An extended version of this work and open-source implementation of EllipseLIO will be presented in a subsequent publication. Future work will integrate visual information into EllipseLIO so that the resulting approach can provide reliable odometry in environments with significant geometric degeneracy where LIO approaches consistently fail.

References

[1] J. Zhang and S. Singh, "LOAM: Lidar Odometry and Mapping in Real-time," in *Robotics: Science and Systems (RSS)*, 2014.

[2] T. Shan *et al.*, "LIO-SAM: Tightly-coupled Lidar Inertial Odometry via Smoothing and Mapping," in *IEEE International Conference on Intelligent Robots and Systems (IROS)*, 2020.

[3] W. Xu and F. Zhang, "FAST-LIO: A Fast, Robust LiDAR-inertial Odometry Package by Tightly-Coupled Iterated Kalman Filter," *IEEE Robotics and Automation Letters (RAL)*, vol. 6, 2020.

[4] W. Xu, Y. Cai, D. He, J. Lin, and F. Zhang, "FAST-LIO2: Fast Direct LiDAR-inertial Odometry," *IEEE Transactions on Robotics (TRO)*, vol. 38, 2021.

[5] K. Chen, R. Nemiroff, and B. T. Lopez, "Direct LiDAR-Inertial Odometry: Lightweight LIO with Continuous-Time Motion Correction," in *IEEE International Conference on Robotics and Automation (ICRA)*, 2023.

[6] Z. Chen, Y. Xu, S. Yuan, and L. Xie, "iG-LIO: An Incremental GICP-Based Tightly-Coupled LiDAR-Inertial Odometry," *IEEE Robotics and Automation Letters (RAL)*, vol. 9, 2024.

[7] H. Lim, D. Kim, B. Kim, and H. Myung, "AdaLIO: Robust Adaptive LiDAR-Inertial Odometry in Degenerate Indoor Environments," in *International Conference on Ubiquitous Robots*, 2023.

[8] A. V. Segal, D. Haehnel, and S. Thrun, "Generalized-ICP," in *Robotics: Science and Systems (RSS)*, 2009.

[9] S. Zhao, H. Zhang, P. Wang, L. Nogueira, and S. Scherer, "Super Odometry: IMU-centric LiDAR-Visual-Inertial Estimator for Challenging Environments," *IEEE International Conference on Intelligent Robots and Systems (IROS)*, pp. 8729–8736, 2021.

[10] D. Lee, H. Lim, and S. Han, "GenZ-ICP: Generalizable and Degeneracy-Robust LiDAR Odometry Using an Adaptive Weighting," *IEEE Robotics and Automation Letters (RAL)*, vol. 10, 2024.

[11] T.-M. Nguyen, D. Duberg, P. Jensfelt, S. Yuan, and L. Xie, "SLICT: Multi-input Multi-scale Surfel-Based Lidar-Inertial Continuous-Time Odometry and Mapping," *IEEE Robotics and Automation Letters (RAL)*, 2022.

[12] M. Ramezani *et al.*, "Wildcat: Online Continuous-Time 3D Lidar-Inertial SLAM," *arXiv*, 2022.

[13] J. Zhu, H. Li, Z. Wang, S. Wang, and T. Zhang, "i-Octree: A Fast, Lightweight, and Dynamic Octree for Proximity Search," in *IEEE International Conference on Robotics and Automation (ICRA)*, 2024.

[14] M. Labussiere, J. Laconte, and F. Pomerleau, "Geometry Preserving Sampling Method Based on Spectral Decomposition for Large-Scale Environments," *Frontiers in Robotics and AI*, vol. 7, 2020.

[15] S. Zhao *et al.*, "SuperLoc: The Key to Robust LiDAR-Inertial Localization Lies in Predicting Alignment Risks," in *IEEE International Conference on Robotics and Automation (ICRA)*, 2025.

[16] M. Ramezani *et al.*, "The Newer College Dataset: Handheld LiDAR, Inertial and Vision with Ground Truth," in *IEEE International Conference on Intelligent Robots and Systems (IROS)*, 2020.

[17] L. Zhang, M. Camurri, D. Wisth, and M. Fallon, "Multi-Camera LiDAR Inertial Extension to the Newer College Dataset," *arXiv*, 2021.

[18] Y. Tao *et al.*, "The Oxford Spires Dataset: Benchmarking Large-Scale LiDAR Visual Localisation, Reconstruction and Radiance Field Methods," *International Journal of Robotics Research (IJRR)*, 2025.

[19] Y. Liu *et al.*, "BotanicGarden: A High-Quality Dataset for Robot Navigation in Unstructured Natural Environments," *IEEE Robotics and Automation Letters (RAL)*, vol. 9, 2024.

[20] Y. Zhu, Y. Kong, Y. Jie, S. Xu, and H. Cheng, "GRACO: A Multimodal Dataset for Ground and Aerial Cooperative Localization and Mapping," *IEEE Robotics and Automation Letters (RAL)*, vol. 8, 2023.

[21] Z. Chen *et al.*, "Heterogeneous LiDAR dataset for benchmarking robust localization in diverse degenerate scenarios," *International Journal of Robotics Research (IJRR)*, 2025.

[22] M. Grupp, *evo: Python package for the evaluation of odometry and SLAM*, 2017. https://github.com/MichaelGrupp/evo.